

General Disclaimer

One or more of the Following Statements may affect this Document

- This document has been reproduced from the best copy furnished by the organizational source. It is being released in the interest of making available as much information as possible.
- This document may contain data, which exceeds the sheet parameters. It was furnished in this condition by the organizational source and is the best copy available.
- This document may contain tone-on-tone or color graphs, charts and/or pictures, which have been reproduced in black and white.
- This document is paginated as submitted by the original source.
- Portions of this document are not fully legible due to the historical nature of some of the material. However, it is the best reproduction available from the original submission.

NASA TECHNICAL MEMORANDUM

NASA TM-82405

THE MSFC VECTOR MAGNETOGRAPH

By M. J. Hagyard, N. P. Cumings,
and E. A. West
Space Sciences Laboratory

February 1981



NASA

*George C. Marshall Space Flight Center
Marshall Space Flight Center, Alabama*

(NASA-TM-82405) THE MSFC VECTOR
MAGNETOGRAPH (NASA) 41 p HC A03/MF AC1
CSCI 03B

N82-27210

Unclas
G3/92 28077


1. REPORT NO. NASA TM-82405		2. GOVERNMENT ACCESSION NO.		3. RECIPIENT'S CATALOG NO.	
4. TITLE AND SUBTITLE The MSFC Vector Magnetograph				5. REPORT DATE February 1981	
				6. PERFORMING ORGANIZATION CODE	
7. AUTHOR(S) M. J. Hagyard, N. P. Cumings, and E. A. West				8. PERFORMING ORGANIZATION REPORT #	
9. PERFORMING ORGANIZATION NAME AND ADDRESS George C. Marshall Space Flight Center Marshall Space Flight Center, Alabama 35812				10. WORK UNIT NO.	
				11. CONTRACT OR GRANT NO.	
12. SPONSORING AGENCY NAME AND ADDRESS National Aeronautics and Space Administration Washington, D. C. 20546				13. TYPE OF REPORT & PERIOD COVERED Technical Memorandum	
				14. SPONSORING AGENCY CODE	
15. SUPPLEMENTARY NOTES Prepared by Space Sciences Laboratory, Science and Engineering Directorate					
16. ABSTRACT <p>The NASA/Marshall Space Flight Center's solar vector magnetograph system is described; this system allows measurements of all components of the Sun's photospheric magnetic field over a 5×5 or 2.5×2.5 arc min square field of view with an optimum time resolution of approximately 100 sec and an optimum signal-to-noise of approximately 1000. The basic system components are described, including the optics, detector, digital system, and associated electronics. Automatic sequencing and control functions are outlined as well as manual selections of system parameters which afford unique system flexibility. Results of system calibration and performance are presented, including linearity, dynamic range, uniformity, spatial and spectral resolutions, signal-to-noise, electro-optical retardation and polarization calibration.</p>					
17. KEY WORDS Solar vector magnetograph			18. DISTRIBUTION STATEMENT Unclassified--Unlimited 		
19. SECURITY CLASSIF. (of this report) Unclassified		20. SECURITY CLASSIF. (of this page) Unclassified		21. NO. OF PAGES 41	22. PRICE NTIS

TABLE OF CONTENTS

	Page
I. INTRODUCTION	1
II. SYSTEM DESCRIPTION	1
A. Optical System	1
B. Camera System	3
C. Sequencing and Control Electronics	5
D. Data Recording and Storage	7
E. Auxiliary Systems	8
III. SYSTEM CALIBRATION AND PERFORMANCE	10
A. Linearity	10
B. Dynamic Range	10
C. Geometrical Distortion	13
D. Uniformity	13
E. Lag	13
F. Resolution	13
G. Signal-to-Noise	16
H. Zeiss Filter Performance Characteristics	18
I. Retardation Measurements	20
J. Polarization Calibration	28
APPENDIX	29
REFERENCES	31

PRECEDING PAGE BLANK NOT FILMED

LIST OF ILLUSTRATIONS

Figure	Title	Page
1	Schematic diagram of the optical system	2
2	Block diagram of the camera system	4
3	Light transfer characteristics of the system's SEC vidicon tube	11
4	Linear response characteristics of the system. a. Response of greyscale generator. b., c., d. System response to generator input as a function of a/d bias	12
5	Digital response of system to a 1956 RETMA chart	14
6	Photograph of uniformly illuminated faceplate of system's SEC vidicon	14
7	Normalized intensity scans across center of the SEC tube in horizontal and vertical directions	15
8	Digital response of system to a Westinghouse resolution chart	17
9	Experimental and theoretical transmission profiles for the 1/8 A-bandpass Zeiss birefringent spectral filter ...	19
10	Relative orientations of the KD*P retarders' slow axes and polarizer-analyzer axis with respect to image plane coordinates (Earth north and east)	21
11	Theoretical variations in KD*P retardation over 2.5 x 2.5 and 5 x 5 arc min field of view	25
12	Measured errors in retardation of KD*P _{1,2} over 5 x 5 arc min field; positive (negative) contours delineate +5 degree (-5 degree) error intervals increasing outward from center. a. KD*P ₂ at + λ/4. b. KD*P ₁ at + λ/4	27
13	Measured errors in KD*P retardations with MgF ₂ correction plate; contours are same as in Figure 12. a. KD*P ₂ at + λ/4. b. KD*P ₁ at + λ/4	28

LIST OF ILLUSTRATIONS (Concluded)

Figure	Title	Page
14	Measured linear variation of KD*P halfwave retardation voltage with temperature for two (A,B) KD*P crystals	29
15	Measured linear polarization compared with expected (theoretical) values	31

LIST OF TABLES

Table	Title	Page
1	Signal-To-Noise Test Results	18
2	Operational Sequencing of Electro-Optical Retarders	23
3	Cross-Talk Analysis Tests	23
4	Method for Retardation Calculations	24
5	Retardation Measurement Results	24

TECHNICAL MEMORANDUM

THE MSFC VECTOR MAGNETOGRAPH

I. INTRODUCTION

The NASA/Marshall Space Flight Center (MSFC) vector magnetograph system originated as a joint effort between the Naval Research Laboratory and MSFC with the objective of building and operating a ground-based instrument located at MSFC which measures vector magnetic fields in active regions on the Sun. The original design of the instrument was the concept of Dr. Guenther Brueckner of the Naval Research Laboratory. Initial operation of the magnetograph began in May 1973 in support of the Skylab/Apollo Telescope Mount missions. After the completion of the Skylab missions, the system underwent extensive redesign and modification in order that the original system specifications might be achieved. Upon completion of this phase of the development, measurements of the full vector magnetic field were initiated in the spring of 1976, and these observations have continued since that time. The magnetograph is currently operated on a daily basis to acquire magnetic field data in collaboration with the Solar Maximum Mission Ultraviolet Spectrometer Polarimeter (SMM UVSP) experiment as part of the SMM Guest Investigator Program (GIP); magnetic field data are also provided on a daily basis to the SMM Experiment Operations Facility (EOF) and the NOAA Forecast Center. In this report we present a description of the system and discuss its calibration and performance characteristics.

II. SYSTEM DESCRIPTION

The measurement of solar vector magnetic fields with the MSFC magnetograph is based on the interpretation of observations of linearly and circularly polarized intensities of a Zeeman-sensitive absorption line selected by a narrow-bandpass birefringent filter. Accordingly, the primary components of the magnetograph are the optical system composed of a light collector, polarization analyzer and filter; camera system; digital system; and, finally, associated electronics.

A. Optical System

The optical train of the MSFC vector magnetograph is shown in Figure 1. Attached to the front of a 30 cm Cassegrainian telescope is a full aperture prefilter with a half width of 21 nm centered at 525 nm and peak transmission of 65 percent at 525 nm. The f/13 Cassegrainian telescope focuses the 30 arc min Sun 38 cm behind the main mirror with an image diameter of 3.5 cm. A mirrored aperture stop at the focus limits

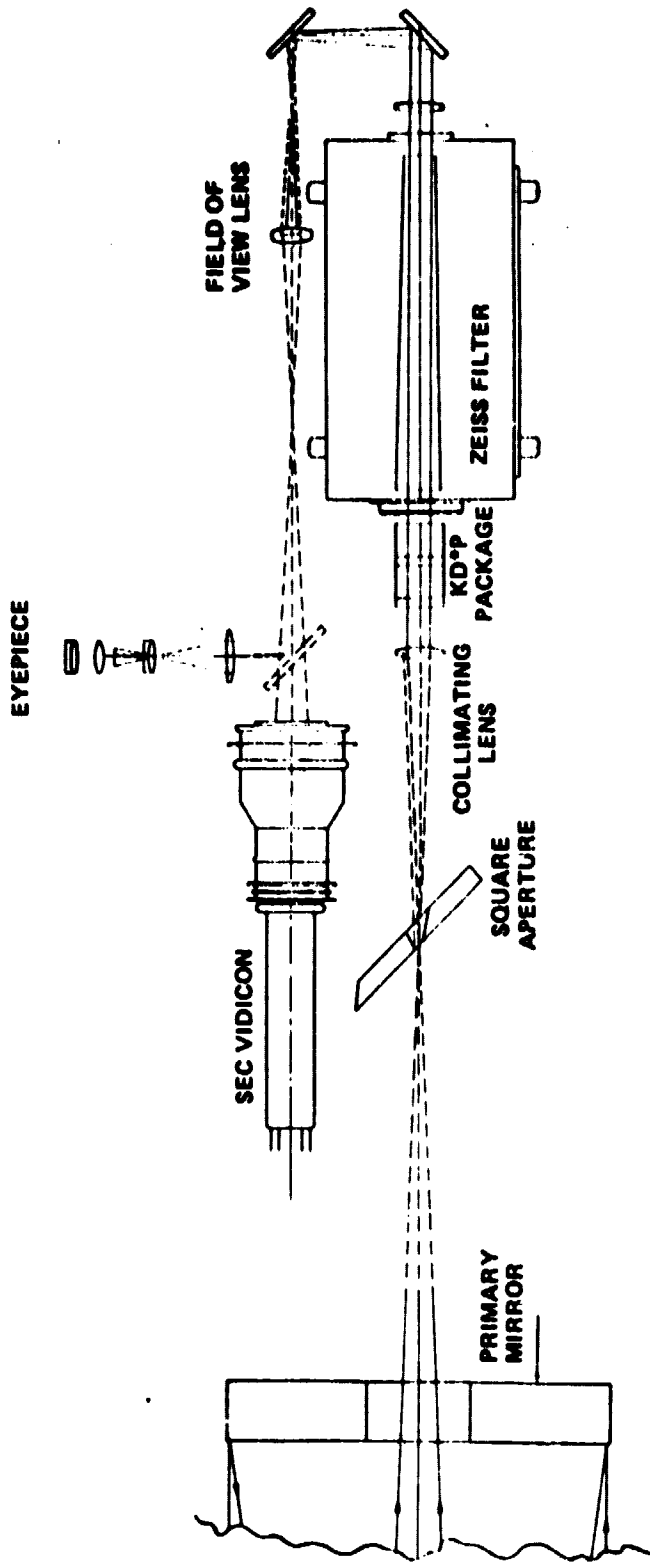


Figure 1. Schematic diagram of the optical system.

the field of view of the Sun to 5×5 arc min (square aperture size 5.9×5.9 mm), reflecting the unused image out of the optics box where it is intercepted by the correlation tracker optics (see Section II.E.3). Following the aperture stop is a collimating lens that insures that the cone angle for the beam passing through the polarizing optics is smaller than 2 degrees. The polarizing optics consist of two KD*P (potassium deuterium phosphate) crystals, a MgF_2 (magnesium fluoride) crystal, and a Zeiss birefringent filter. The optic axes of the KD*P crystals and MgF_2 crystal are aligned parallel to the light beam. The KD*P crystals are used as variable waveplates, and the MgF_2 crystal is used to extend the acceptance angle of the two KD*P crystals to 2 degrees. The first polarizing element of the Zeiss birefringent filter is used as the analyzer of the system. The Zeiss filter is a 0.012 nm bandwidth filter centered on the FE I line, 525 nm, and can be tuned ± 0.800 nm. The light transmitted by the Zeiss filter is folded around the optics box and through a lens system consisting of two independent and exchangeable magnification systems which refocus a 5×5 arc min or 2×2 arc min field of view of the Sun onto a Secondary Electron Conduction (SEC) vidicon tube.

B. Camera System

The camera system consists of an SEC detector, associated signal conditioning electronics, and the system memory; a block diagram is shown in Figure 2.

1. Detector

The selected field of view is imaged by the optics on an SEC camera tube, Westinghouse type WL 31439 with a fiber optics faceplate. The useful diameter of the tube is 40 mm, allowing a 28×28 mm image to be formed. The SEC tube was picked for its high signal gain, excellent storage properties, and low residual retention of the stored signal after a single scan of the reading beam. The tube consists of an S-20 photocathode, an electrically focused diode image section, an SEC target and a magnetically focused and deflected reading section. Alignment coils located in the deflection assembly are used to improve the flatness of the video image. The horizontal and vertical alignment coils are connected to a dc voltage source which is controlled by a potentiometer, thereby affording a continuously variable control of the alignment coil current. The magnetically deflected reading section scans the SEC target in 128 discrete horizontal steps along 128 discrete lines.

2. Electronics

The signal from the SEC tube is coupled directly into the video preamplifier. This preamplifier was designed specifically to match the SEC vidicon tube characteristics utilizing a special low-noise, field-effect transistor as the input device. To keep the output noise as low as possible, the preamp has a relatively narrow bandpass of only 300 kHz, providing for an equivalent noise level of only 175 pA; the overall gain of the preamp is 10^6 - (V out)/(A in).

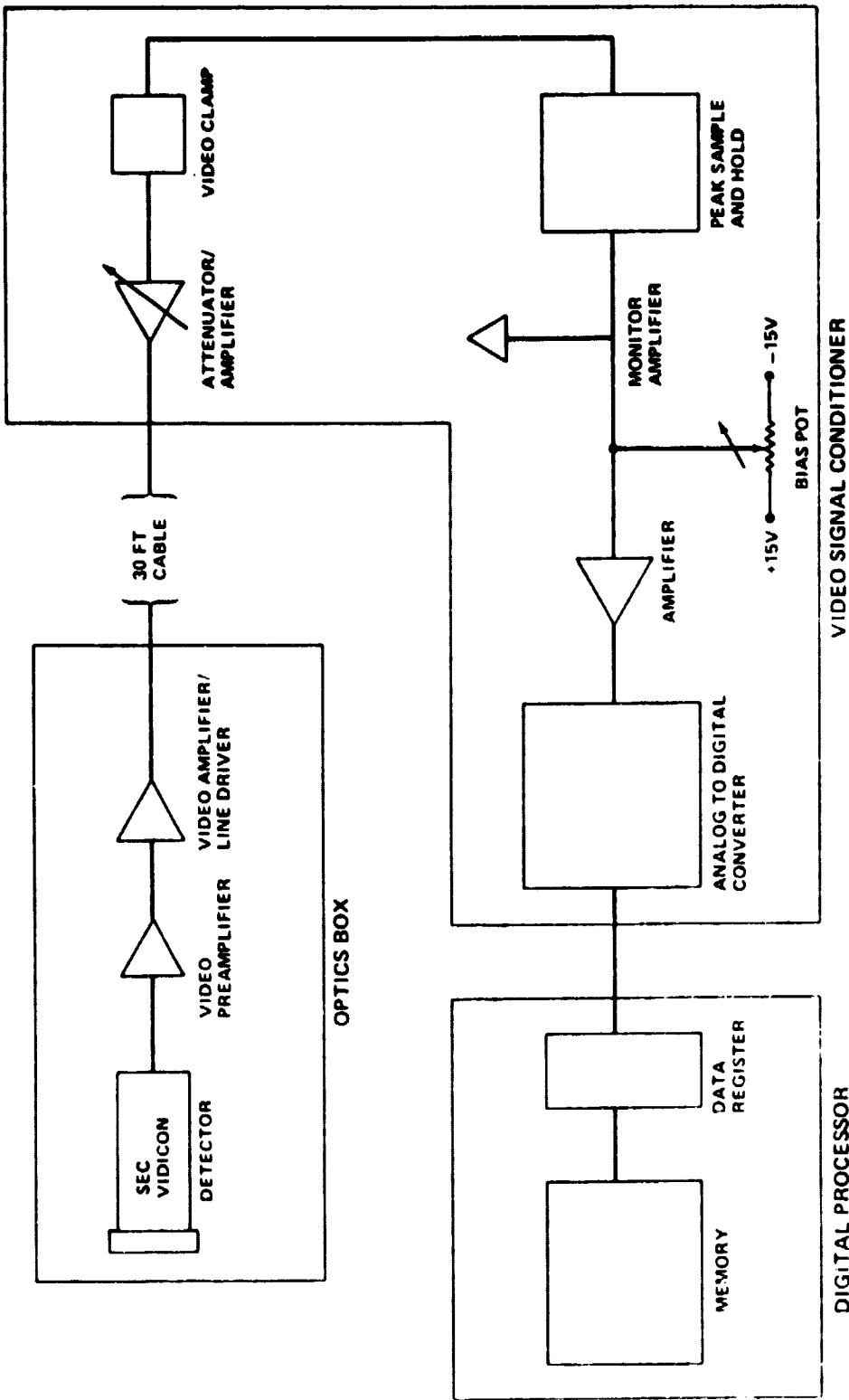


Figure 2. Block diagram of the camera system.

A video amplifier and line driver are located in the optics box to amplify the video signal and drive the approximately 30 ft of coaxial cable between the optics box and the video signal conditioner located at the control rack. The amplifier has a bandwidth of 1 MHz, and input and output impedances of 100 ohms and 50 ohms, respectively. A ten-step attenuator/amplifier is used to adjust the video signal to the optimum level required by the digitizing electronics; this amplifier is of the same design as the video amplifier. The optimized signal passes into a dc restoration circuit consisting of a keyed clamp and a wideband video amplifier. The clamp keeps the dc level of the data at zero volts so that there is no smearing between picture elements under extreme contrast conditions.

A peak sample and hold circuit retains the peak value of each picture element for 1.2 μ s to allow a complete digital conversion of the analog signal by the analog-to-digital (a/d) converter. As a result, the peak accuracy of the signal can be determined to within 99 percent. The a/d converter is a Datel high-speed system which converts the signal level of each element into an 8-bit digital word. A bias pot and amplifier located at the input to the a/d can be adjusted to set the dc level into the a/d to 0 V. The 8-bit a/d converter has an input voltage of 0 V to -5.0 V full scale, an encode rate of 1.25 MHz, a conversion time of 100 ns/bit, and an accuracy of one part in 256. A video amplifier located at the output of the peak sample and hold circuit provides a video signal for the analog display monitor.

The output of the a/d is clocked into a data register where it is converted from serial to parallel and put into memory. This memory, a microram 3400 semiconductor system built by Electronic Memories and Magnetics Corporation, is used for data storage and preprocessing. This memory has a capacity of 16 k \times 32 bits, a 275 ns access time, and a 900 ns read/modify/write timing cycle. It can store two 128 \times 128 images (A,B) simultaneously with word size variable from 8 to 16 bits depending on the number of images (maximum of 255) superimposed; selector switches allow the operator to select from the total 16-bit word the 8 bits to be displayed.

C. Sequencing and Control Electronics

The sequencing and control logic of the magnetograph is provided by a controller which was designed and fabricated by Electro-Mechanical Research, Inc. (EMR). The controller provides all timing signals, the horizontal and vertical sync pulses for the camera and displays, driver logic for the KD*P crystals and Zeiss filter, memory control logic, addition and subtraction logic, memory input and output registers, and data transfer logic.

In addition to the automatic sequencing and control functions cited previously, the controller also affords a great deal of flexibility for the magnetograph system by providing for the automatic selection by the operator of various system parameters as discussed in the following subsections.

1. Dynamic Range

Variation of the photocathode voltage of the SEC tube provides a gain control range of 15:1 which is determined by the operating voltage range of 3.5 to 7.5 kV. Additional system dynamic range can be obtained by changing the exposure times and attenuator/amplifier settings: six exposure times can be selected ranging from 1/60 s to 1/1.875 s, and the attenuator/amplifier has 10 steps, each changing the signal gain by 10 percent.

2. Signal-to-Noise

To obtain an increased signal-to-noise ratio, the data can be digitally enhanced by a process of superimposing successive data from opposite polarization pairs (A, B) in the two memory registers. Enhancement control switches allow the operator to select the number of enhancements in one-step intervals from 1 to 255. Operating at 1/60 s exposure time, the full 255 enhancements of a polarization pair (A, B) can be obtained and recorded in 35 s.

3. Filter Wavelength Selection

The operator can tune the Zeiss birefringent filter over the wavelength interval $5250.2 \text{ \AA} \pm 5.0 \text{ \AA}$ in steps of 10 mÅ. Control is provided by four independent thumbwheel selector switches and, as a consequence, four different filter positions can be preprogrammed and quickly selected.

4. Polarization Analysis Sequences

The selection of the voltages applied to the KD*P electro-optical modulators can be made manually by the operator, or automatic sequences of voltages can be chosen. The manual selection is employed generally in the installation, alignment and testing of the electro-optical modulators, whereas the automatic modes are selected in the general magnetograph operation. In the automatic mode five different sequences are available, corresponding to five different polarization analyses:

- 1) Left and right circular polarization (1A, 1B);
- 2) Linear polarization at 45° and 135° to the analyzer (2A, 2B);
- 3) Linear polarization at 0° and 90° to the analyzer (3A, 3B);
- 4) 2. and 3. in sequence;
- 5) 1., 2., and 3. in sequence.

5. SEC Target Signal Retention

The beam-discharge lag which is inherent in all scanning electron-beam devices results in the retention of approximately 15 percent of the information on the vidicon. To reduce errors introduced by this lag, the sequencing and control electronics can be preset so that the tube is

rescanned by the read-beam without target exposure. This rescan without exposure can be performed up to seven times; however, three rescans are usually sufficient, and over-erasure can charge the target negatively, with a resulting reduced signal in the next exposure [1, 2].

A different target characteristic of the SEC which can introduce errors into the data is the presence of image charge patterns within the SEC target layer which are not neutralized by the readout beam. As a result, the target signal of the first exposure in a data set may be up to 10 percent greater than subsequent signals, and the percentage increase is directly dependent on the elapsed time between data sets. While regeneration is presumably not a problem in SEC tubes [3], this "bleeding" problem has been encountered previously [4] and the increased target signal has been explained by McMullan and Towler [5]. The different SEC vidicons that have been used in the MSFC magnetograph system have displayed varying degrees of "bleeding"; the tube presently in the system exhibits this effect to a small degree. To circumvent the problem entirely, the control electronics have been modified to automatically reject the first exposure in the A and B frames so that these data are not put into the memory.

D. Data Recording and Storage

The magnetograph system uses a microcomputer to process data stored in the microram memory. These data are initially stored on a 5-megabyte cartridge disk; once data acquisition is complete, the data are transferred to magnetic tape for permanent storage and input to other computers for data reduction and analysis. The system consists of an LSI-11/2 microprocessor with hardware floating point, real-time clock and bootstrap, 64 kilobytes of dynamic ram memory, a 10-megabyte disk drive (5 fixed, 5 removable), an ADM-3 terminal, a four-port serial interface (DLV11-J), 2 parallel interface boards (DRV11), and a special interface board designed to provide communication with the solar magnetograph system.

The LSI-11/2 microprocessor controls the data acquisition and magnetic tape output. The 64K dynamic memory is used for program and data storage and is the largest memory configuration available for the LSI/11-2. The terminator board contains the real-time clock and the bootstrap. The disk drive has a fixed platter of 5-megabyte capacity and a provision for 1 cartridge disk of 5 megabytes of removable storage. Each cartridge can hold approximately 74 double frames (A, B) of solar magnetograph data.

The ADM-3 terminal is used for operator control of the system. It provides a display of 24 lines of 80 characters each and a keyboard. Interface is through the serial interface board (1 port). One parallel interface board is used for communication with the solar magnetograph using the special interface and accepts data at a rate of approximately 500 kilobits per s. The second board provides output to the solar magnetograph tape unit.

The special interface board latches the solar magnetograph data and stops the data transfer out of the magnetograph until the LSI-11 reads the data. It also contains cables for sending data to the tape unit and is switch selectable so that direct solar-magnetograph-to-tape data transmission can occur.

The tape recorder is a Digi-Data nine-track recorder with a ping-pong buffer. The buffers are able to read and store data at a 1 megabit/s rate. While one buffer of information is being recorded on tape, the other buffer can be filled. The data are recorded on the tape at 800 bpi, and the buffers will hold 16 kilobits. The direct solar-magnetograph-to-tape data transmission provides an alternate method of recording the data. Although direct recording of the data is approximately a factor of 20 slower, it provides a reliable backup recording system.

E. Auxiliary Systems

1. Test Pattern Generators

Two independent digital signal generators are provided in the system to check out and set up the magnetograph system. A greyscale generator digitally produces 16 levels of grey, each one-half the amplitude of the preceding level and equally spread across the tube format. The generator is capable of producing the grey levels in either horizontal or vertical bars. A flat field also can be produced at the 16 greyscale levels. The signal is synchronized with the magnetograph system using internal sync circuits, amplified to the required signal level by a discrete amplifier, and capacitively coupled directly into the video preamp input. The generator output is linear to less than 0.5 percent full scale; the level can be varied either continuously or in discrete steps. A checkerboard generator produces a symmetrical checkerboard pattern of 16 bits off and 16 bits on, alternating every 16 lines. The pattern is inserted into the digital portion of the system, allowing checkout of the memory and its associated digital circuits.

2. Solar Guider

The solar tracking system for the MSFC magnetograph is a unique system which was designed, fabricated, and installed inhouse at MSFC. The system consists of a Sun sensor, torque motor drivers and associated electronics. The Sun sensor, a spare sensor manufactured by Ball Brothers Co. for the Lunar Roving Vehicle program, is a two-axis sensor using two detectors for each axis and a fifth detector as an intensity sensor for automatic gain control. The sensor field of view is ± 6 degrees with a nonlinearity of approximately 1 percent over the range of ± 0.5 degree. The torque motors, built by Inland Motor Co., produce 1.9 ft lb per amp with a peak torque of 22 ft lb. To keep the motors in a safe operating range, the supply voltage limits the torque to 14 ft lb. The

motor tachometers produce 22 V/rad/s with a ripple voltage of ± 0.49 percent. By installing low-friction Kaydon ABEC Class 7 ball bearings in the telescope mount, the drive friction was reduced to less than 5 ft lb. With a well-balanced telescope, 14 ft lb of torque is more than adequate to drive the telescope.

The detector output for each axis, which is proportional to the off-set error between the sensor block pointing axis and the solar vector, is amplified in the first stage of the electronics and then AGC'd with the output of the intensity sensor to maintain a gradient of 10 mV/s. This signal is summed with the tachometer signal. Tachometer feedback is used to achieve the required gain bandwidth. The error signal drives a current source power amplifier with a gain of 10 A/V.

Through calibration, the sensor can be made to point to any given spot on the Sun by dialing an offset voltage which is summed with the AGC'd output. The torquer will drive the gimbal until the output of the sensor forces the error signal caused by the offset voltage to be zero. The AGC maintains the position regardless of changes in intensity. The nonlinearity of the AGC is less than ± 0.5 percent. The combined nonlinearity of the AGC and the sensor fix the accuracy of defining or locating a spot to approximately 15 arc s. The loop gain at dc is essentially infinite, so that the average tracking error of any spot is zero. The jitter stability about any spot with little or no wind is approximately ± 2 arc s.

Upon initial turn-on, the system can be put into an acquisition mode by a panel switch. This opens the Sun loop and allows the gimbals to be driven to the sensor f.o.v. at a controlled rate by the offset pointing potentiometers. When the Sun is in the f.o.v. of the sensor as indicated by the intensity meter, the system is switched to the automatic tracking mode. In the automatic tracking mode the system will track with no variations in performance over an intensity range of 10 to 100 percent. Below 10 percent an intensity threshold monitor opens the tracking loop and places the system in a hold mode until the intensity increases above 10 percent. To prevent damage to the telescope or the telescope drive motors, an overspeed sensing device located in both axes will sense an abnormally fast movement of the telescope and will turn off the telescope drive power. Power can be reset by turning off the acquisition switch and turning it back on.

3. Correlation Tracker

While the guider system's jitter stability is approximately ± 2 arc s with little or no wind loading, frequently wind conditions at the MSFC observing site produce significant high-frequency oscillations which the guider system cannot handle. To stabilize these motions a solar correlation tracker [6] has been integrated into the magnetograph system. This correlation tracker compensates for image motion using error signals derived from a video correlation technique; the error signals drive a flat optical element to translate the image to the original unperturbed position. Tests have been conducted with this instrument in operation during magnetograph observations to assure that no spurious linear polarization is introduced into the data by the flat plate.

III. SYSTEM CALIBRATION AND PERFORMANCE

Prior to installing the SEC vidicon which is presently in operation in the magnetograph, an extensive testing program was conducted to document its performance in the system. In Sections III.A through III.G we discuss results of these tests, in III.H we discuss performance characteristics of the Zeiss filter, and in III.I and III.J we present results of polarization analyses and calibrations.

A. Linearity

The light transfer characteristics of the tube were measured to insure that the vidicon is operated in the linear portion of the transfer curve. The light source used in this test was a calibrated optoliner with a set of neutral density filters to accurately measure the light level at the SEC faceplate. The data shown in Figure 3 indicate that the light transfer is linear when the tube is operated at a signal current output of less than 100 nA. In normal operation, the high-voltage power supply for the vidicon is adjusted such that maximum solar illumination corresponds to approximately 100 nA; consequently, all intensity variations measured over the field of view will fall on the linear portion of the transfer curve.

To test the linear response of the system apart from the vidicon, the greyscale generator described in Section II.E.1 was used. In Figure 4a measurements of the linearity of the generator alone are shown, and in Figure 4b, c, and d, the responses of the system to the generator input signals are shown for various levels of the a/d bias.

B. Dynamic Range

The scene-to-scene dynamic range of the system is determined primarily by the 15:1 gain control range achieved by varying the photocathode voltage from 3.5 to 7.5 kV, by the 32:1 range in exposure times, and by the $(255)^{1/2}$:1 range in picture enhancements.

The range of illumination which can be accommodated by the tube within a single scene is roughly from 10^{-5} to 10^{-3} footcandle (within the linear portion of the light transfer curve); this range of ≈ 100 :1 is consistent with measurements of the tube signal-to-noise of 41 db as described in Section III.G. The dynamic range of the complete system is determined by the overall signal-to-noise of the system, which is ≈ 100 :1 (see Section III.G); this value provides more than sufficient range to accommodate the radiance variations in a solar scene which range from umbral to photospheric intensities. Experimental verification of this is derived from measured intensities taken on 24 November 1976, for active region 757 (Boulder Number). The minimum magnetograph signal in the umbral region was 2189 counts, while the average photospheric signal was measured to be 11650; the resulting umbral-photospheric intensity ratio of 0.188 is consistent with quoted values of ≈ 0.2 for this ratio (e.g., Ref. 7).

ORIGINAL PAGE IS
OF POOR QUALITY

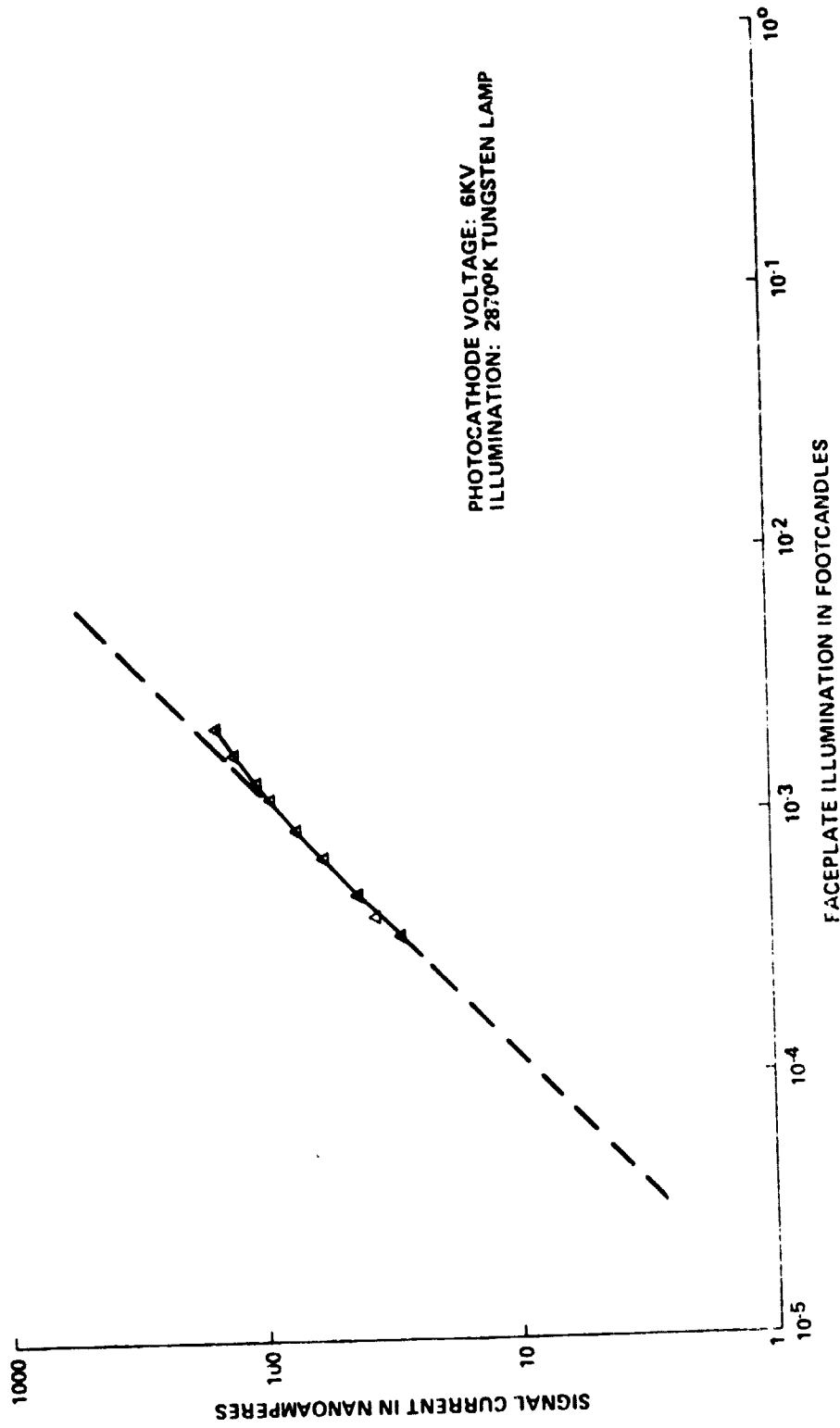


Figure 3. Light transfer characteristics of the system's SEC vidicon tube.

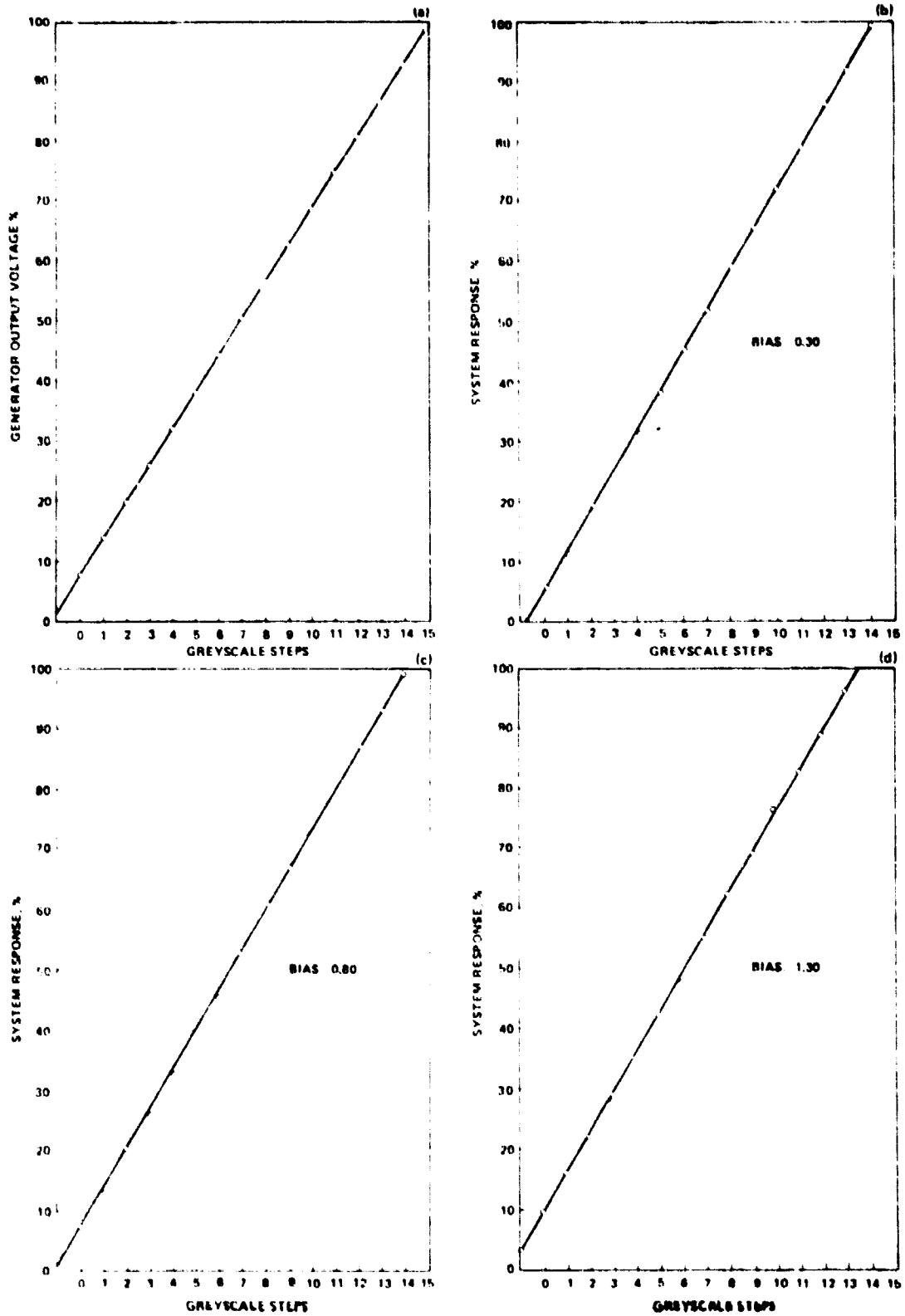


Figure 4. Linear response characteristics of the system.
a. Response of greyscale generator. b., c., d. System response to generator input as a function of a/d bias.

C. Geometrical Distortion

The geometrical distortion of the vidicon was investigated by illuminating the faceplate with a 1956 RETMA chart. A photograph of the system's digital reproduction of this image is shown in Figure 5; from this it can be concluded that there is negligible geometrical distortion in the image.

D. Uniformity

The Westinghouse specifications for the uniformity of the SEC camera tube presently installed in the magnetograph indicate a variation of 20 percent from center to edge; Figure 6 is the manufacturer's target quality photograph showing a uniformly illuminated faceplate. To experimentally determine uniformity of the SEC tube and telescope optical system, a defocussed, 5×5 arc min area of the quiet Sun near disk center was used for uniform illumination of the faceplate. In Figure 7a and b normalized intensity distributions from digitized data measured across the center of the tube in both horizontal and vertical directions are shown to indicate system uniformity. These data indicate that in the vertical direction, the uniformity is within ± 10 percent over 90 percent of the center of the tube and the signal intensity begins to roll off rapidly as the edge of the scan area is approached. In the horizontal direction the tube is flat within ± 10 percent over 80 percent of the tube, again rolling off rapidly toward the edge.

E. Lag

The second and third field lags in the SEC vidicon were measured by exposing the tube to obtain the normal operating signal level, turning off the photocathode voltage so that no additional signal could reach the target, and reading the tube three consecutive times. The signal level of the second readout was approximately 15 percent of the level of the first readout, and the third was 5 percent of the first. The second and third field lags are then 15 and 5 percent, respectively.

F. Resolution

The resolution of the SEC vidicon which is quoted by Westinghouse is 700 TV lines per raster height. The resolution of the magnetograph system, however, is determined by the system raster of 128 lines in the vertical direction and by the 128 discrete elements in the horizontal direction. Using the Kell factor [8] of 0.70, the system's resolution is equivalent to 90 lines/raster height and 90 elements/line. Therefore, for the 5×5 arc min field of view the spatial resolution of a magnetogram is 3.3 arc s; for the 2×2 arc min field it is 1.3 arc s.

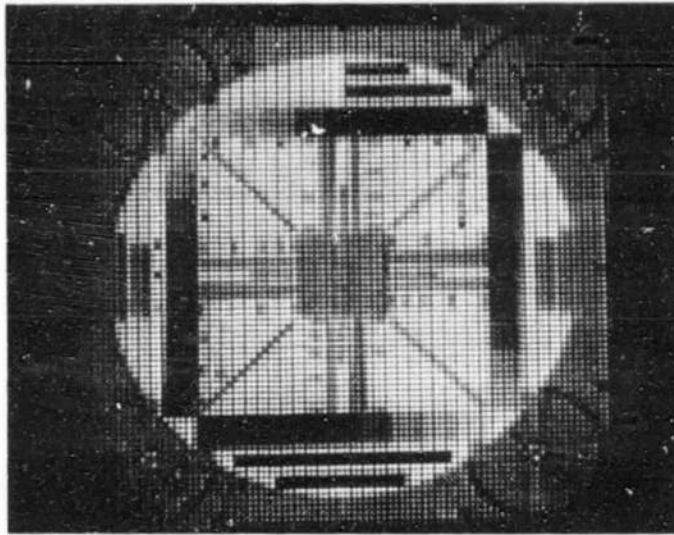


Figure 5. Digital response of system to a 1956 RETMA chart.

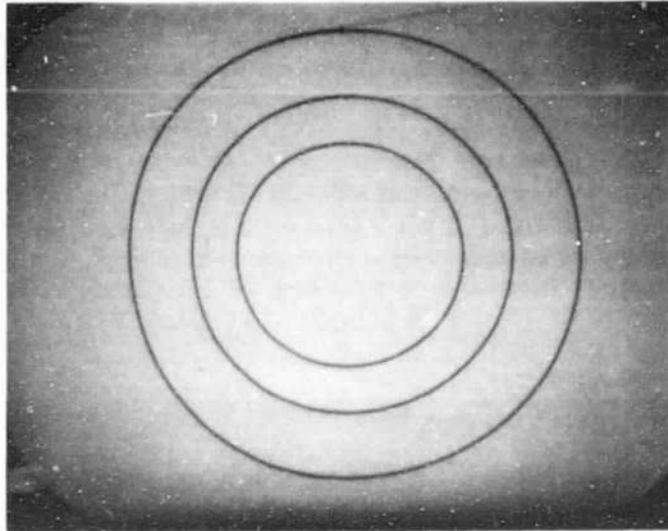


Figure 6. TV display of uniformly illuminated faceplate of system's SEC vidicon.

ORIGINAL PAGE
BLACK AND WHITE PHOTOGRAPH

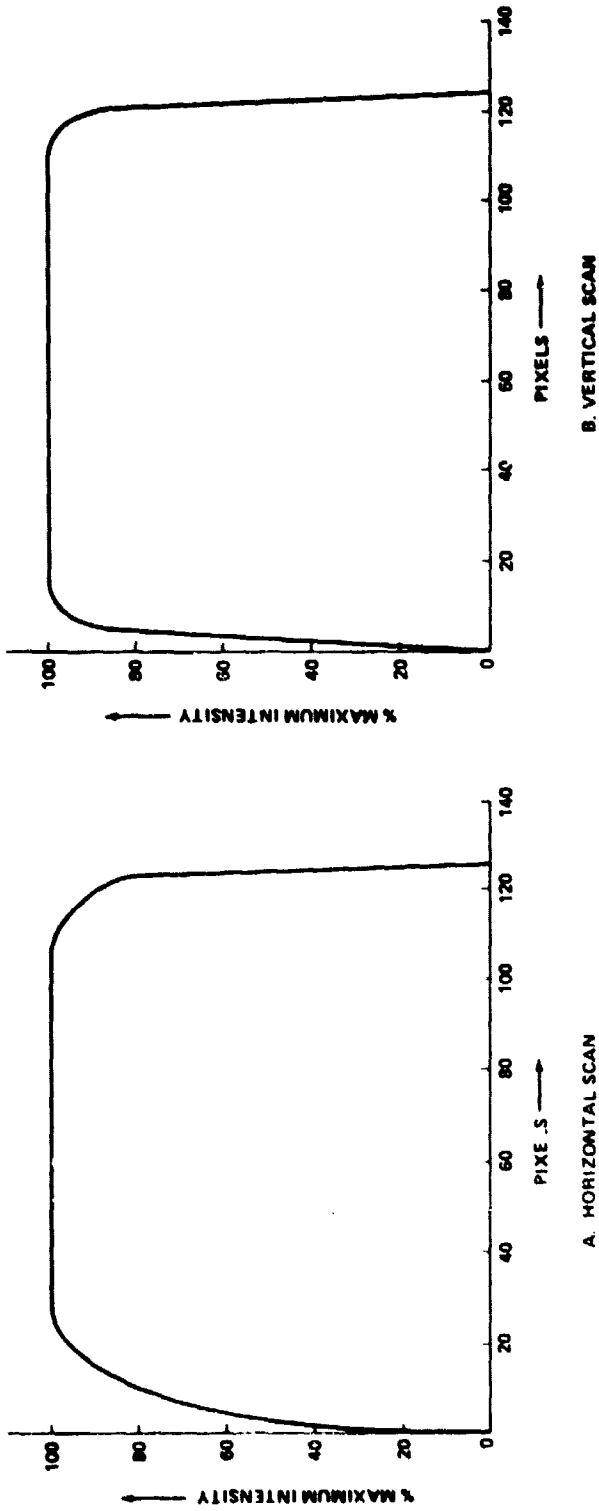


Figure 7. Normalized intensity scans across center of the SEC tube in horizontal and vertical directions.

In Figure 8, a photograph of the Westinghouse resolution chart shows that light bars which are two elements or greater in width can be resolved easily. As the bar width approaches the size of an individual element, the resolution of the bar is determined by its position relative to the center of the element: lines falling on the center of elements are clearly resolvable, whereas those falling between elements are not resolved.

G. Signal-to-Noise

Theoretical calculations of the signal-to-noise ratios (S/N) of the various components of the analog and digital systems can be made using known techniques, and from these individual S/N values the system's overall S/N can be estimated. As an example, the SEC vidicon S/N is calculated from the number of photoelectrons (n) produced per picture element (pixel) per exposure:

$$(S/N)_{\text{sec}} = n / (n)^{1/2} .$$

The value of n is estimated from the expected photon flux ϕ :

$$\phi = I_{\odot} \times T \times B \times A \times a ,$$

where I_{\odot} is the solar radiation, T is the transmission of the Earth's atmosphere and of the filter and optics, B is the filter bandpass, A is the collecting area of the telescope's primary mirror, and a is the area of the solar surface represented by one pixel at λ 5250. With

$I_{\odot} = 1.8 \times 10^{11}$ photons/s [$\text{m}^2 \cdot \text{\AA} \cdot (\text{arc s})^2$], $T \approx 0.01$, $B = 1/8 \text{ \AA}$, $A = 0.073 \text{ m}^2$ (for a 0.30 m primary aperture) and $a = 2.5 \times 2.5 (\text{arc s})^2$, we have

$$\phi = 1.03 \times 10^8 \text{ photons/s}$$

incident on each pixel. For a quantum efficiency of 1/10 and an exposure time of 1/60 s, we calculate a value for the number of photoelectrons, n , equal to 1.71×10^5 ; consequently, we have $(S/N)_{\text{sec}} = 414$.

For the preamplifier the estimated rms noise level is 175 pA (Section II.B.2) and the upper limit for the signal current is 100 nA, so that for this component the S/N is given by

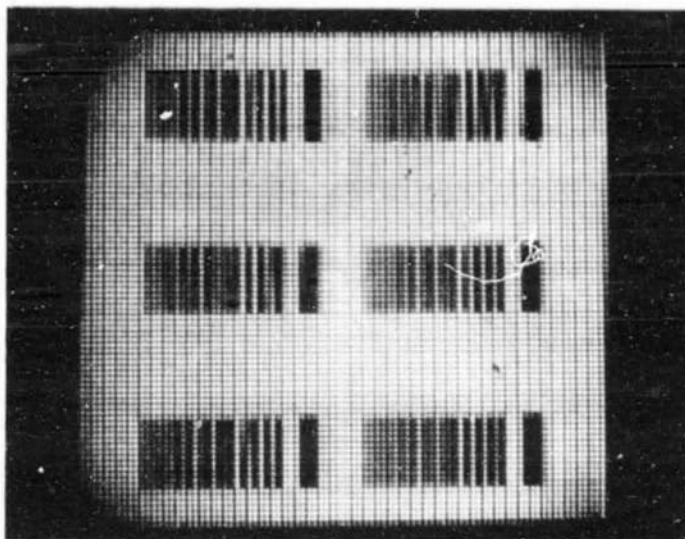


Figure 8. Digital response of system to a Westinghouse resolution chart.

$$(S/N)_p = 100 \text{ nA} / 175 \text{ pA} = 570 \quad .$$

The theoretical equivalent S/N for both the vidicon and preamp thus would be on the order of 335. However, experience teaches us that the actual value of a system's S/N can be quite different from the theoretical estimate and that this theoretical value usually serves only as an upper limit. In fact, the S/N of the camera and preamplifier was measured experimentally at the output of the camera video amplifier using the composite video signal. The light level at the vidicon faceplate was adjusted to yield a 100 nA output signal current. The output signal voltage and noise voltage were measured to be 1.5 V and 75 mV peak to peak, respectively. Using the formula [9]

$$S/N = 6 (CE-CD)/CD$$

where CE and CD are the signal and noise envelopes, respectively, the resultant S/N is 114:1 or 41 db.

Other components in the magnetograph system will add to the noise, and for some of these it is difficult to estimate a S/N factor. Consequently, we have devised an experimental technique from which we can determine the S/N of the total system and which can be used periodically to monitor the S/N status. In this technique, we assume that the noise level from each pixel derives from two distinct sources: a true random

(rms) noise and a "fixed pattern" noise caused by the variation of response of the vidicon target surface (nonuniformity across the vidicon). In the Appendix we derive analytical expressions used to calculate the magnitudes of these two noise sources from experimental measurements that are made periodically under varying conditions of the system's status; generally the data are taken with the KD*P crystals in the off mode and the telescope defocused on a quiet solar area. In Table 1 we present results of some of these periodic tests which indicate a nominal value of $\sim 100:1$ when operating voltages are optimized.

TABLE 1. SIGNAL-TO-NOISE TEST RESULTS

<u>Date</u>	<u>Status</u>	<u>S</u>	<u>N</u>	<u>S/N</u>
10/02/75	5250	230	2.16	106
	Continuum	216	2.13	101
11/01/76	5250	374	3.86	97
		373	3.98	94
03/16/77	5250	314	2.09	150
03/22/77	SEC Cathode Voltage = 3200V, gain = 2	377	7.17	53
	SEC Cathode Voltage = 3600V, gain = 1	290	3.52	82
	SEC Cathode Voltage = 3800V, gain = 1	339	3.23	105

H. Zeiss Filter Performance Characteristics

To analyze the states of linear and circular polarization over a narrow wavelength interval of the 525.022 nm (5250.22 Å) solar absorption line, the MSFC magnetograph system utilizes a specially built Zeiss birefringent filter designed to have a bandpass of 0.0125 nm (125 mÅ) at 525.022 nm. In December 1968 and again in May 1975 experimental verification of the optical characteristics of the Zeiss filter were undertaken by members of the Space Sciences Laboratory (SSL) and Dr. William Livingston and his associates of the Kitt Peak National Observatory using the McMath solar telescope and spectrograph; the data obtained from these experiments were reduced and analyzed by members of SSL. Photoelectric scans of the filter transmission near the center of the Zeiss aperture were obtained with the Zeiss filter tuned to 525.120 nm (5251.20 Å) in the solar continuum; the filter was then tuned to line center, 525.022 nm (5250.22 Å), where further photoelectric scans were obtained. From these data the experimental transmission profile of the filter was derived and is shown in Figure 9. Further results indicate that the transmission profile for the full aperture is quite similar to this and there are no appreciable changes in filter transmission characteristics as the filter is tuned over its entire range of 525.022 nm \pm 0.80 nm. The theoretical transmission of a birefringent filter composed of N elements is given by

ORIGINAL PAGE IS
OF POOR QUALITY

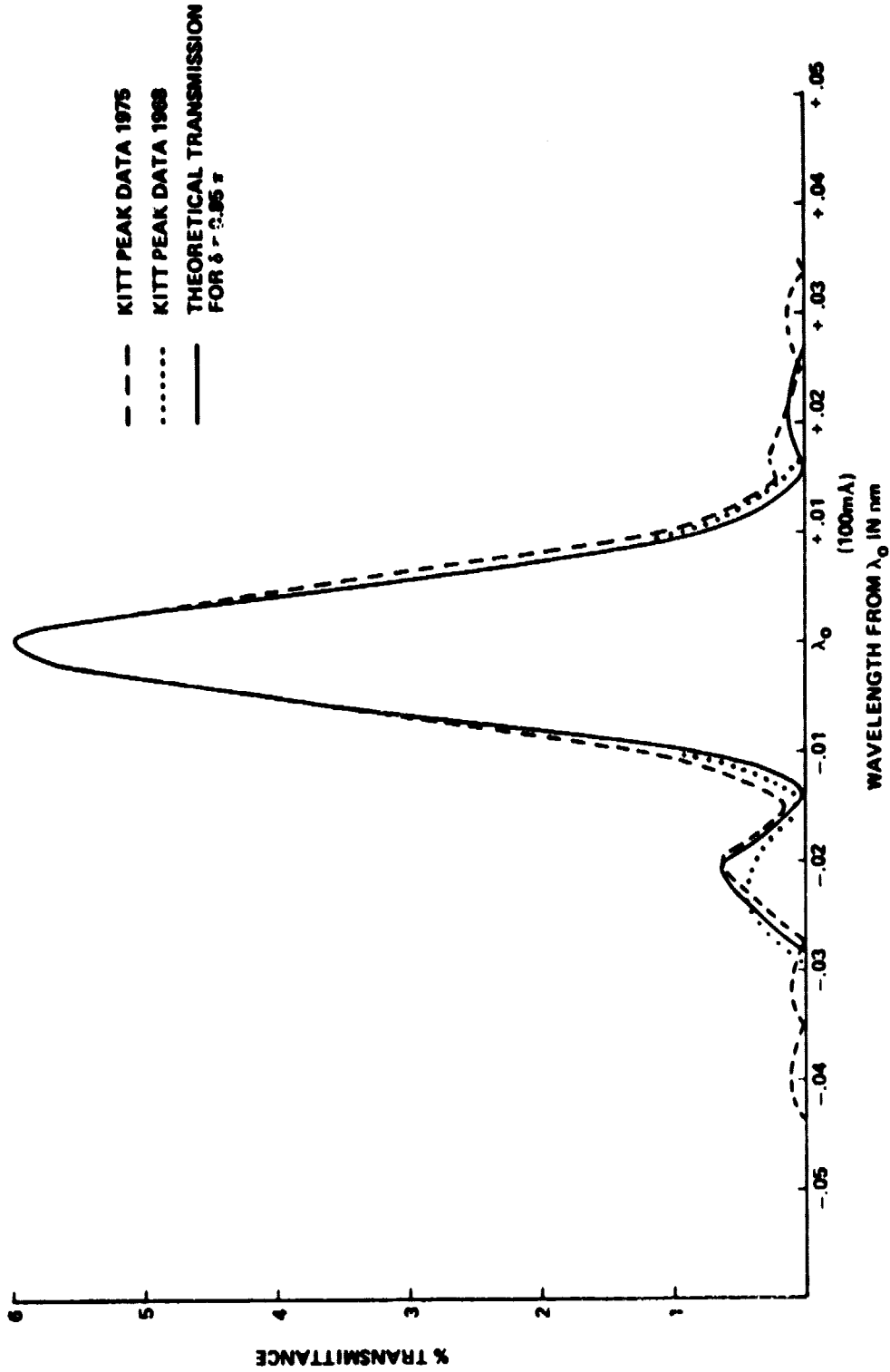


Figure 9. Experimental and theoretical transmission profiles for the 1/8 A-bandpass Zeiss birefringent spectral filter.

$$T = T_0 \prod_{k=0}^N [\cos(\pi \Delta \lambda 2^{-k} d^{-1})]^2 ,$$

where T_0 is the transmission at the center wavelength (λ_0) of the bandpass, T is the transmission at a wavelength λ , $\Delta \lambda = \lambda - \lambda_0$, and d is a constant. If the final polarizing element of the filter is rotated through an angle δ , the transmission characteristics are then determined by the equation

$$T' = T [\cos(\pi \Delta \lambda d^{-1} + \delta)]^2 .$$

By choosing $\delta = 0.85 \pi$, a good fit to the experimental transmission profile is obtained, as is indicated in Figure 9. This analytical representation for the Zeiss filter has thus been adopted for use in computer programs for the reduction and interpretation of the magnetograph data.

I. Retardation Measurements

The basic principle of operation of the MSFC magnetograph is the accurate analysis of the state of polarization of the incident solar intensity. This analysis is accomplished by introducing known retardations into the optical path by means of the two electro-optical crystals (KD*P's). Consequently, it is important to determine experimentally the performance status of the KD*P's and to ascertain that each crystal is producing as nearly as possible the correct retardation in each of the six measurement sequences. In this section we outline the experimental techniques developed for these purposes and present results of several tests. In Figure 10, the relative orientation of the slow (s) axes of the two KD*P retarders together with the polarizing plane of the analyzer (A) are shown in the x, y, z coordinate system where +z represents the direction of light propagation in the optical train. The analyzer (A), which is the first polarizing element of the Zeiss birefringent filter, has its transmission axis oriented at 20 degrees from the +x axis; the slow axis of KD*P₁ is parallel to this direction, while that of the second KD*P is rotated 45 degrees from it. The axis x_0 designates a reference direction determined by the orientation of the transverse component of the measured solar magnetic field. In the analysis the three basic types of polarized light (Q, U, V) are defined in relation to the analyzer axis (A). The intensities +Q and +U represent linear polarizations parallel and at 45 degrees to A, while +V and -V represent right and left circular polarizations, respectively; these three parameters (Q, U, V) together with the total intensity, I, comprise the Stokes vector which completely describes the intensity and state of polarization of a beam of light. In the six operational sequences of the MSFC magnetograph, the six polarized intensities +V, -V, +Q, -Q, +U and -U are transformed via the electro-optical retarders into light

ORIGINAL PAGE IS
OF POOR QUALITY

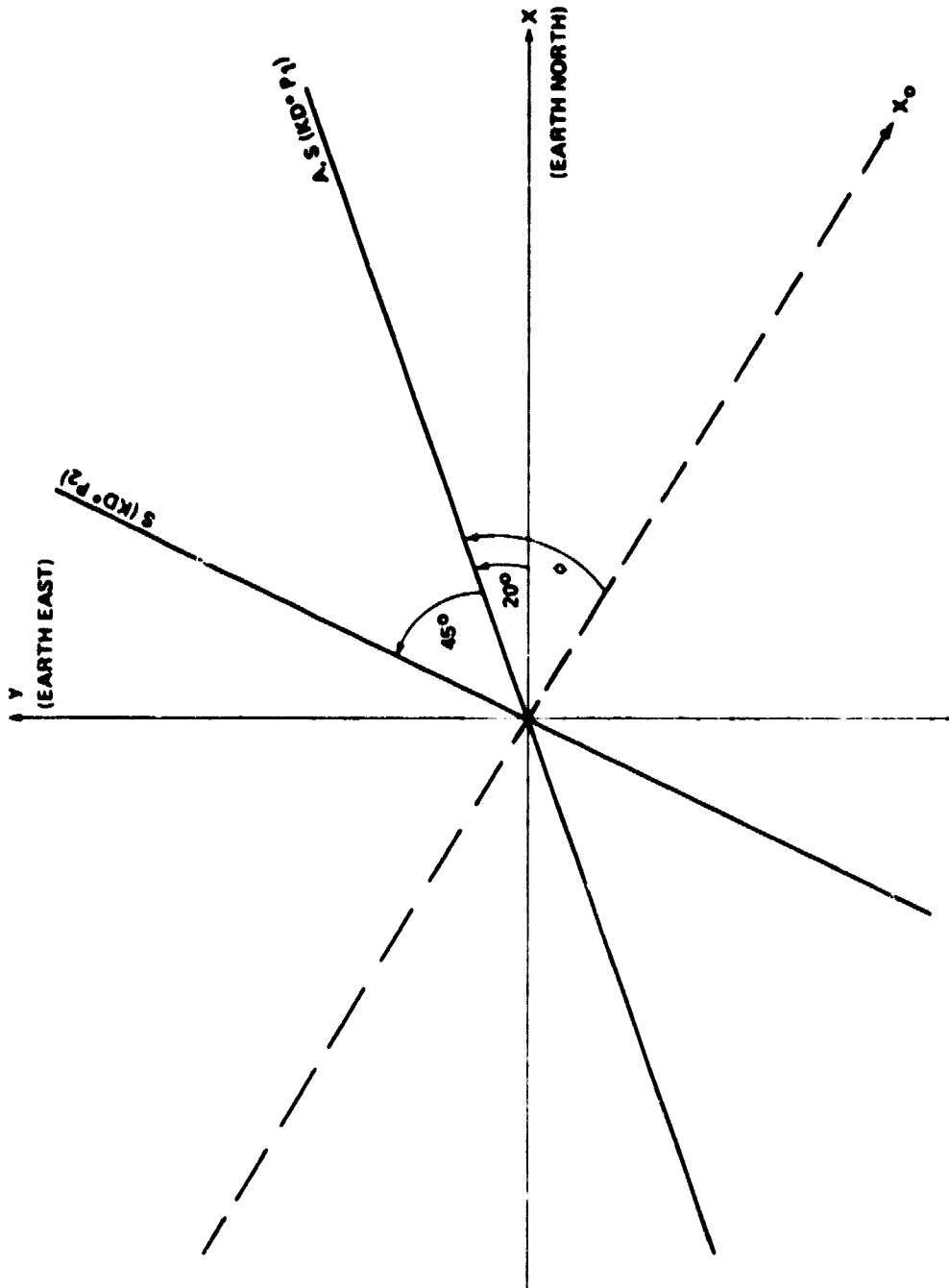


Figure 10. Relative orientations of the KD#P retarders' slow axes and polarizer-analyzer axis with respect to image plane coordinates (Earth north and east).

intensities linearly polarized parallel to the analyzer transmission axis; in this manner the complete polarization analysis of the incident beam is performed. This polarization analysis can be expressed mathematically by use of the Mueller matrices [10] for the two KD*P retarders and the linear analyzer. If the retardations of the crystals KD*P₁ and KD*P₂ are designated δ_1 and δ_2 , respectively, and if the linear analyzer's transmission axis is at an angle ϕ to the reference direction x_0 , then the measured intensity in the *i*th sequence is given by

$$\begin{aligned}
 I_i = & 1/2 \{ I + Q_0 [\cos(\delta_2)_i \cos 2\phi - \sin(\delta_1)_i \cdot \sin(\delta_2)_i \cdot \sin 2\phi] \\
 & + U_0 [\cos(\delta_2)_i \sin 2\phi + \sin(\delta_1)_i \sin(\delta_2)_i \cos 2\phi] \\
 & + V_0 [\cos(\delta_1)_i \sin(\delta_2)_i] \}, i = 1, 2, \dots, 6 .
 \end{aligned} \tag{1}$$

In this equation the Stokes parameters for linear polarization, Q_0 and U_0 , are defined with respect to the directions x_0 and z in Figure 10. In Table 2 we show a hypothetical "analysis" in which it is assumed the retarders perform perfectly; the six sequences represent the actual operational sequences of the MSFC system, but the retardations $(\delta_1)_i$ and $(\delta_2)_i$ actually introduced by the KD*P's generally vary from the quoted values. To complete this hypothetical analysis the case of a homogeneous magnetic field must be assumed so that the Stokes parameter U_0 may be set to zero [11], and the parameters I , Q_0 and V_0 as well as the azimuth ϕ can be calculated readily from sums and differences of the I_i .

In actual practice the analysis can be complicated by variations of the retardances $(\delta_1)_i$ and $(\delta_2)_i$ from their specified values. Thus, it is necessary to measure the actual retardances introduced and their variations over the field of view. This is accomplished by operating the system in the six sequences while introducing known states of polarized light into the optical beam with the insertion of a linear polarizer and a quarter-wave plate. If these known polarization states are described relative to the analyzer axis direction A , the transmitted intensity is given by the following expression derived from equation (1) with $\phi = 0$:

$$\begin{aligned}
 I_i = & 1/2 [I + Q \cos (\delta_2)_i + U \sin (\delta_1)_i \sin (\delta_2)_i \\
 & + V \cos (\delta_1)_i \sin (\delta_2)_i] .
 \end{aligned} \tag{2}$$

**ORIGINAL PAGE IS
OF POOR QUALITY**

TABLE 2. OPERATIONAL SEQUENCING OF ELECTRO-OPTICAL RETARDERS

Sequence (i)	KD*P ₁	KD*P ₂	(δ_1) _i	(δ_2) _i	I _i
1	OFF	+ $\lambda/4$	0°	+90°	1/2 (I + V _o)
2	OFF	- $\lambda/4$	0°	-90°	1/2 (I - V _o)
3	+ $\lambda/4$	+ $\lambda/4$	90°	+90°	1/2 (I - Q _o sin 2 ϕ + U _o cos 2 ϕ)
4	+ $\lambda/4$	- $\lambda/4$	90°	-90°	1/2 (I + Q _o sin 2 ϕ - U _o cos 2 ϕ)
5	OFF	OFF	0°	0°	1/2 (I + Q _o cos 2 ϕ + U _o sin 2 ϕ)
6	OFF	$\lambda/2$	0°	180°	1/2 (I - Q _o cos 2 ϕ - U _o sin 2 ϕ)

Using this expression we can analyze the measured intensities of the six operational sequences of the system (Table 2) in each of the six experimental tests performed in this "cross-talk" analysis as outlined in Table 3.

TABLE 3. CROSS-TALK ANALYSIS TESTS

Test Description	Stokes Parameter	Measured Intensity
1. Linear polarizer parallel to A	+Q	1/2 I [1 ± cos (δ_2) _i] , i=1,...6.
2. Linear polarizer perpendicular to A	-Q	
3. Linear polarizer at +45° to A	+U	1/2 I [1 ± sin (δ_1) _i sin (δ_2) _i] , i=1,...6.
4. Linear polarizer at -45° to A	-U	
5. Linear polarizer at +45° to $\lambda/4$ plate	+V	1/2 I [1 ± cos (δ_1) _i sin (δ_2) _i] , i=1,...6.
6. Linear polarizer at -45° to $\lambda/4$ plate	-V	

Theoretically, from these data the values of (δ_2)_i, i = 1, ..., 6, can be calculated; in practice, however, the data allow accurate calculations only for (δ_2)_{1, 2, 3, 4}. This is a direct consequence of the "stickiness" of the SEC vidicon, a problem which is discussed in Sections II.C.5 and III.E. In sequences 5 and 6 the + and - Q Stokes parameters are measured; in tests 1 and 2 the + and - Q Stokes parameters are experimentally introduced into the optical light path. As a result, the signals in sequences 5 and 6 of these two tests occur in a "high-low" pattern, and, because of the tube "stickiness", the "low" signal is in error and the correct retardations (δ_2)_{5,6} cannot be calculated accurately. Furthermore, this problem also occurs in tests 3, 4, 5, and 6 for their respective "high-low" sequences. Consequently, the scheme outlined in Table 4 has been devised to circumvent the "high-low" problem and still yield calculations for the various retardations.

TABLE 4. METHOD FOR RETARDATION CALCULATIONS

Tests	Calculated Retardations	Remarks
I. 1 & 2	$(\delta_2)_{1,2,3,4}$	—
II. 3 & 4	$(\delta_1)_{1,2, (5,6)}$	Use $(\delta_2)_{1,2}$ calculated in I.
III. 5 & 6	$(\delta_1)_{3,4}$	Use $(\delta_2)_{3,4}$ from I.
IV. 5 & 6	$(\delta_2)_{5,6}$	Assume $(\delta_1)_{5,6} = (\delta_1)_{1,2}$

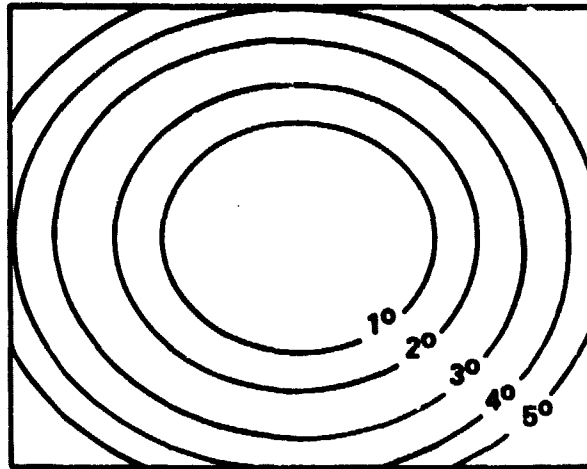
In Table 5 we present typical results of such a calculation scheme obtained on 22 October 1976; the values indicated are obtained from an average of several pixels at the center of the field of view (on the optical axis).

TABLE 5. RETARDATION MEASUREMENT RESULTS

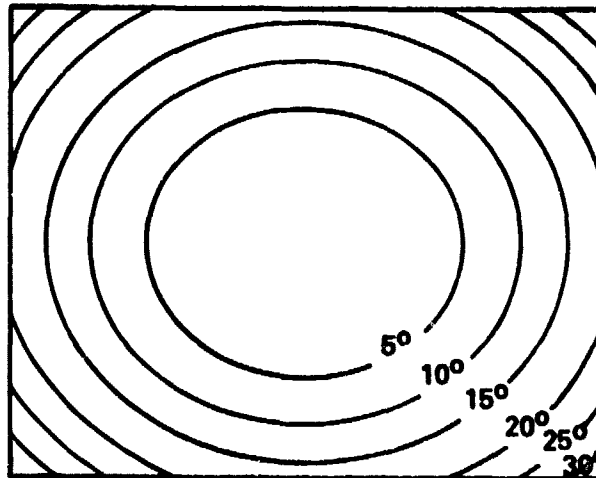
Sequence (i)	δ_1		δ_2	
	Measured	Theoretical	Measured	Theoretical
1	-0°.14	0°	91°.52	+90°
2	+0°.43	0°	-87°.75	-90°
3	87°.81	90°	+90°.20	+90°
4	90°.22	90°	-89°.76	-90°
5	(1)	0°	+2°.73	0°
6	(2)	0°	+177°.89	180°

The excellent agreement between theoretical and measured retardations indicated by these results cannot be obtained over the entire field of view of the MSFC magnetograph. This problem is a consequence of the natural birefringence of the KD*P crystals wherein the phase retardance is different for different optical path lengths through the crystal. For light rays on or near the optic axis of the system, the collimator renders the beam parallel to this axis. However, for off-axis point sources in the 5 x 5 arc min field of view, the light from each point will be collimated but the collimated beams will be inclined relative to each other. Since the optic axes of the KD*P's are aligned experimentally to be perpendicular to the center of the aperture, the maximum deviations in retardances occur from points at the corners of the square field of view. In Figure 11 we show the theoretically calculated variations in retardation over the 2.5 x 2.5 and 5 x 5 arc min fields of view. From retardation

ORIGINAL PAGE IS
OF POOR QUALITY



FIELD OF VIEW 2.5 X 2.5 ARC MIN



FIELD OF VIEW 5X5 ARC MIN

Figure 11. Theoretical variations in KD^*P retardation over 2.5×2.5 and 5×5 arc min field of view.

tests of 22 October 1976, we calculated the errors in retardations of both KD*P crystals in all six sequences. Figure 12 shows contour levels of the retardation errors for KD*P_{1,2} in sequences 3 and 4 (Table 2); positive and negative contours represent ± 5 degree error increments outward from the center of the field of view.

Because of these nonnegligible errors in the retardances away from the center of the field of view, we can see from equation (1) that the data reduction scheme illustrated in Table 2 is no longer valid. The symmetry of the pairs of sequences is lost and the data reduction to obtain I , Q_0 , V_0 , and ϕ (assuming a homogeneous magnetic field where $U_0 = 0$) is at best extremely complicated, especially in view of the large number of individual data points (128×128) which must be analyzed in each sequence. Because of these complications a magnesium fluoride (MgF_2) correction plate has been designed and installed between the two KD*P crystals. Since MgF_2 and KD*P are, respectively, positive and negative uniaxial crystals, the field-of-view errors in retardation introduced by the KD*P can be reduced substantially by a properly designed and aligned MgF_2 plate. In Figure 13 measured contour levels of retardation errors at ± 5 degree increments are again shown for the KD*P sequences of Figure 12, but in this case a MgF_2 correction plate has been added to the KD*P optical package. As can be seen by comparing Figures 12 and 13, the variation of retardance over the 5×5 arc min field of view has been reduced from ± 25 degrees (where the central retardance is 90 degrees) to ± 5 degrees. Consequently, the original data reduction scheme can be used with only small corrections required for the extreme corners of the field of view. A more detailed discussion of how the MgF_2 plate expands the field of view of two KD*P's can be found elsewhere [12].

One final point to be mentioned in this discussion of the performance of the polarizing optics is the temperature dependence of the dc voltage applied to a crystal to obtain a given retardance. This variation is described by the linear relation

$$V_1 = V_{RT} (T_1 - T_c) / (T_{RT} - T_c) ,$$

where V_1 is the halfwave voltage of the KD*P temperature T_1 , V_{RT} is the halfwave voltage at the room temperature T_{RT} , and T_c is the Curie temperature (220° K). In Figure 14 we illustrate this linear variation of voltage with temperature and indicate the experimentally measured data for two different KD*P crystals. To guarantee that the voltages which are applied to the two KD*P crystals during operation of the system produce the correct retardations, the temperature of the crystals must

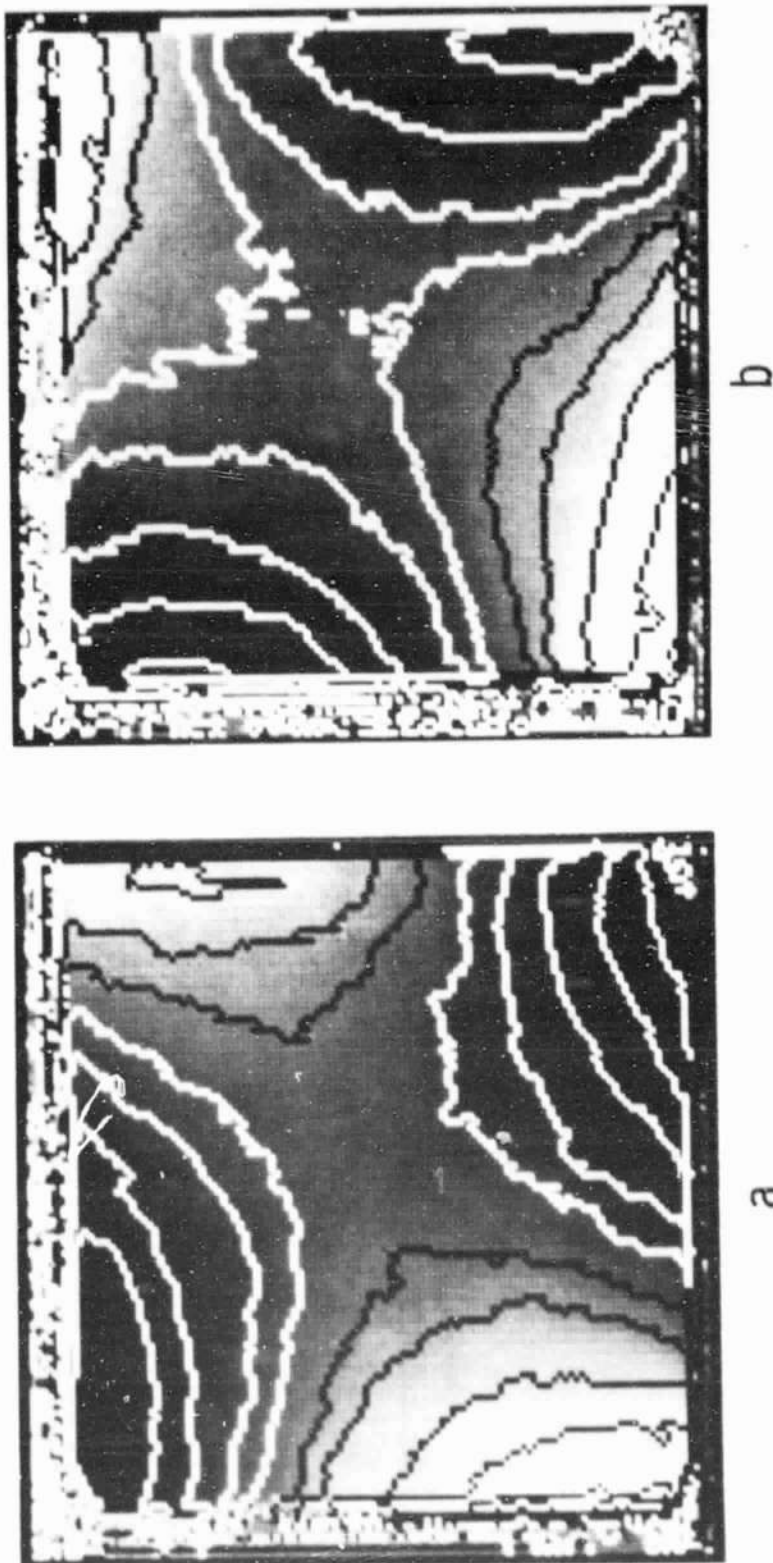
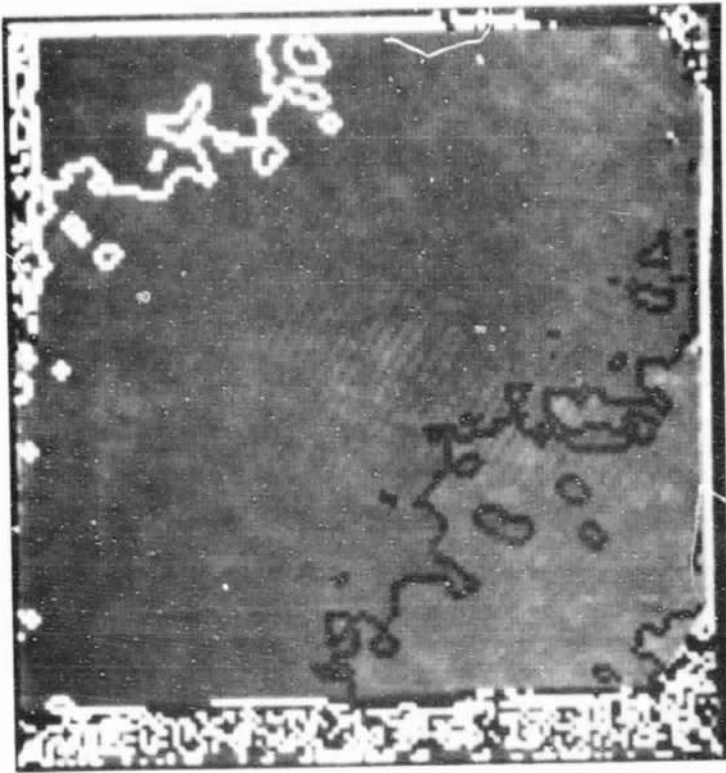
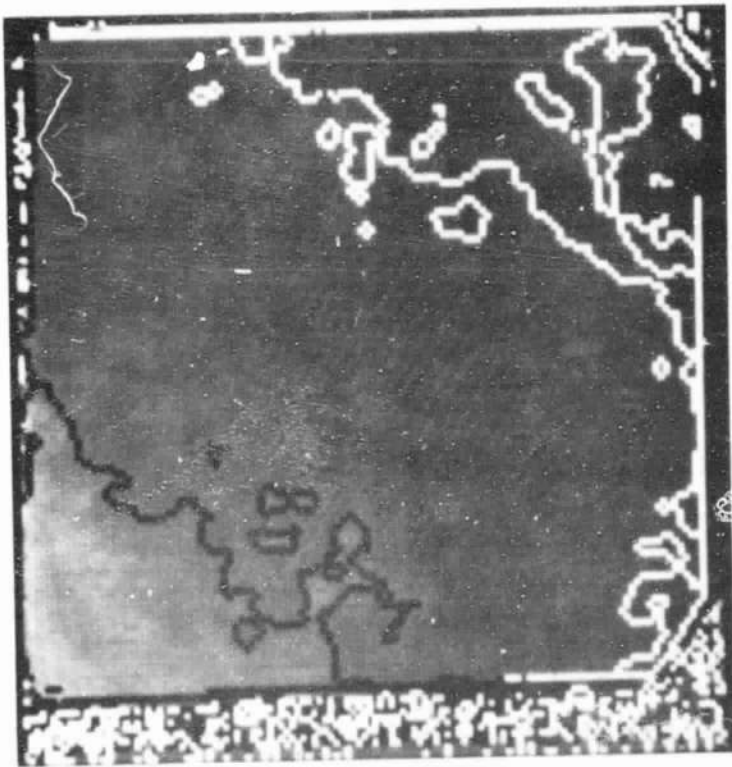


Figure 12. Measured errors in retardation of $KD^*P_{1,2}$ over 5×5 arc min field; positive (negative) contours delineate $+5$ degree (-5 degree) error intervals increasing outward from center. a. KD^*P_2 at $+\lambda/4$. b. KD^*P_1 at $+\lambda/4$.



b



a

Figure 13. Measured errors in KD*P retardations with MgF₂ correction plate; contours are same as in Figure 12. a. KD*P₂ at + $\lambda/4$. b. KD*P₁ at + $\lambda/4$.

ORIGINAL PAGE IS
OF POOR QUALITY

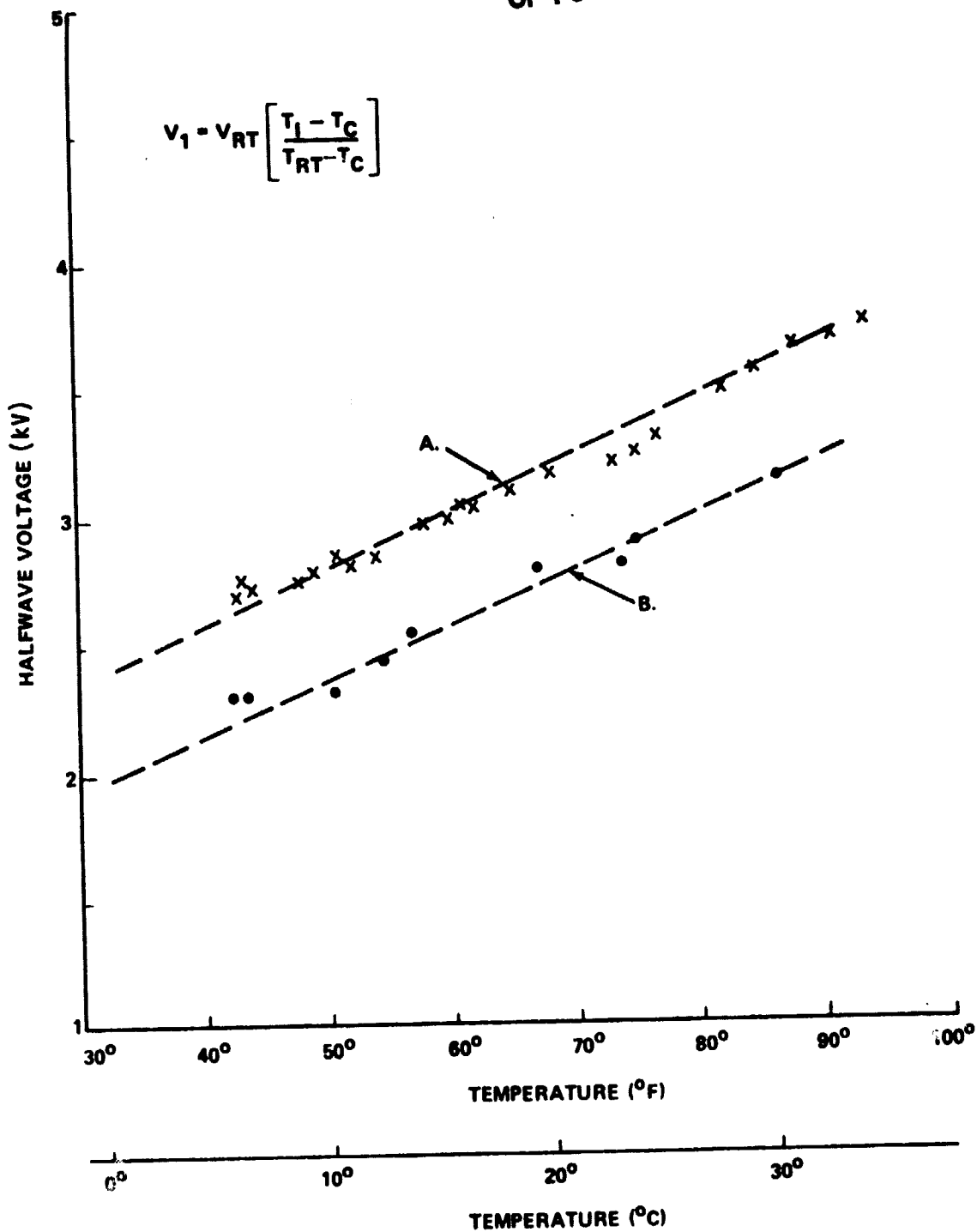


Figure 14. Measured linear variation of KD*P halfwave retardation voltage with temperature for two (A,B) KD*P crystals.

be held constant throughout the observing period. To accomplish this a temperature controller has been built and placed in the optics box. The temperature of the optics box is set at the expected maximum seasonal temperature (75°F winter, 100°F summer). This temperature can be controlled to within $\pm 0.5^\circ\text{F}$. This eliminates the variation of temperature during an observing period while minimizing both the high-voltage requirements for the KD*P's and the thermal gradients in the optics box.

J. Polarization Calibration

The ultimate test of the reliability and accuracy of the MSFC magnetograph system is the comparison of measured polarizations with values expected when known levels of linearly and circularly polarized intensities are introduced into the optical beam. Figure 15 illustrates results obtained for the U and Q Stokes parameters when linear polarization was produced by rotating a polarizer in front of the polarizing optics. Three separate data sets were obtained for each curve representing zero, one and two vidicon re-scans (erasures) between successive exposures. These results indicate the problem of vidicon "stickiness" whereby the measured polarization is only 75 to 80 percent of the expected value for the case of no re-scans. If one re-scan is introduced, in the case of low and intermediate values of percentage polarization, the measured signal is approximately 95 percent of the true value, and this is probably within the accuracy of the experimental technique of producing the polarized light. The saturation of the measured polarization at approximately 87 percent, regardless of the number of re-scans, when 100 percent polarization (theoretically) is introduced, is attributed to residual intensities in the "low" signal due to improper setting of the a/d bias voltage and to incomplete extinction by the crossed polarizers. However, these problems occur for very high levels of percentage polarization which are not encountered in measurements of linear and circular polarizations produced by solar magnetic fields since calculations based on penumbral, plage and photospheric models indicate that polarization levels are limited to 40 percent or less regardless of the magnetic field strength. Thus, results from tests such as these indicate that data taken with no vidicon re-scans will need to be calibrated, but if re-scans are introduced, the measured polarization levels will be reliable. Furthermore, it appears that one re-scan should be sufficient to achieve this degree of reliability.

ORIGINAL PAGE IS
OF POOR QUALITY

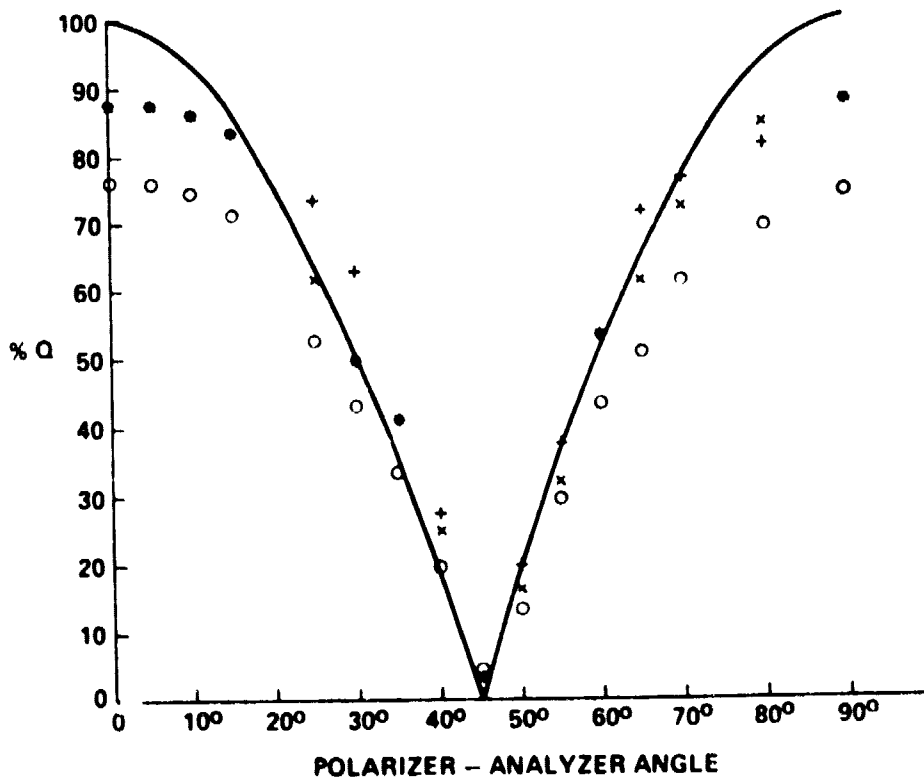
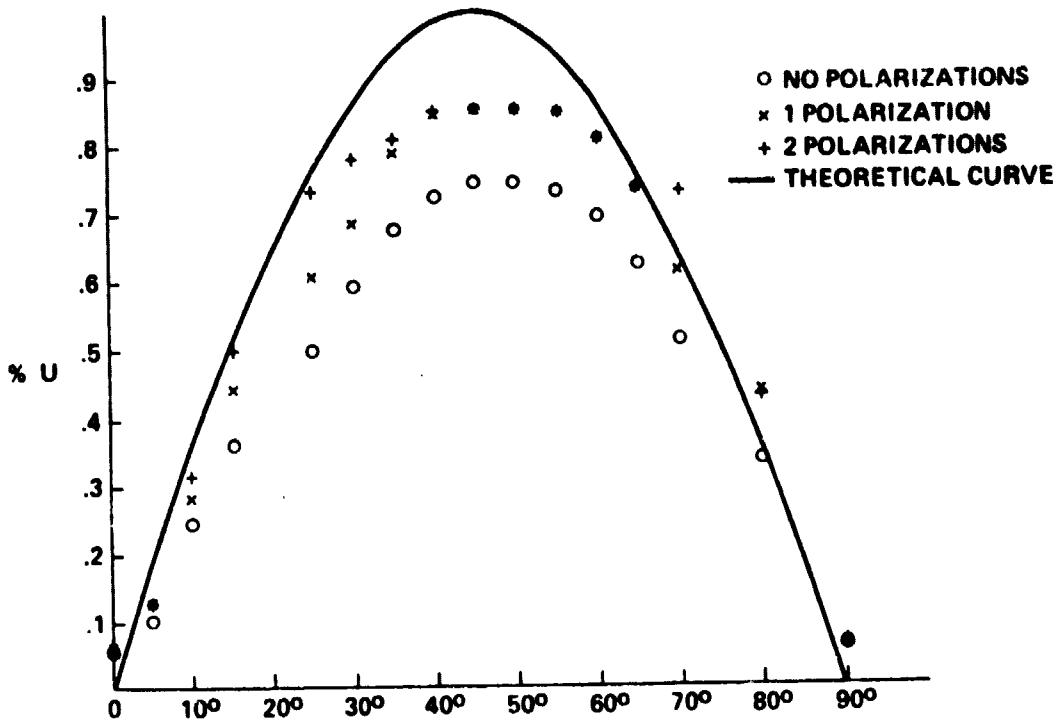


Figure 15. Measured linear polarization compared with expected (theoretical) values.

APPENDIX

In deriving expressions for the random and fixed pattern noise, the following assumptions are made:

1) The fixed pattern noise and the rms noise average to zero over the field of view of 16,384 pixels;

2) After a large number (~ 128) of exposures or enhancements are superimposed, the rms noise at each pixel averages to zero;

3) While the fixed pattern noise at each pixel may vary with intensity, the ratio of this noise to the incident intensity is constant.

If we define the rms noise and fixed pattern noise of the i, j pixel as σ_{ij} and Δ_{ij} respectively, then the recorded signal for this pixel, I_{ij} , for exposure 1 is given by

$$(I_{ij})_1 = I_1 + (\Delta_{ij})_1 + \sigma_{ij} \quad , \quad (A1)$$

where I_1 is the "true" intensity signal. After a number m of exposures have been superimposed, where m is large, the measured signal is

$$(I_{ij})_m = I_m + (\Delta_{ij})_m \quad . \quad (A2)$$

Under our assumptions the averages of $(I_{ij})_1$ and $(I_{ij})_m$ over the field of view (128×128 pixels) are

$$\overline{(I_{ij})_1} = I_1$$

and

$$\overline{(I_{ij})_m} = I_m \quad .$$

Furthermore, assumption (iii) implies the relation

$$(\Delta_{ij})_m / I_m = (\Delta_{ij})_1 / I_1 \quad .$$

It follows, using equation (A2), that

$$(\Delta_{ij})_1 = I_1 (\Delta_{ij})_m / I_m = I_1 \{ (I_{ij})_m / I_m - 1 \} \quad , \quad (A3)$$

and, from equation (A1)

$$\sigma_{ij} = (I_{ij}) - (I_1 / I_m) (I_{ij})_m \quad . \quad (A4)$$

In the actual procedure, measurements are made of the matrices $(I_{ij})_1$ and $(I_{ij})_m$ where m is 128 or 256. From these data the averages

$$\overline{(I_{ij})_1} = I_1$$

and

$$\overline{(I_{ij})_m} = I_m$$

are calculated and, using equations (A3) and (A4), the relative fixed pattern noise $(\Delta_{ij})_1 / I_1$ and random noise σ_{ij} can be computed. From the rms value of σ_{ij} , the system signal-to-noise can be calculated with the signal given by I_m / m .

REFERENCES

1. R. K. Honeycutt and M. S. Burkhead: Adaptation of a Commercial Silicon Vidicon Detector System for Astronomical Spectroscopy. Astronomical Observations with Television-Type Sensors, Proceedings of Symposium at University of British Columbia, Vancouver, B. C., Canada. J. W. Glaspey and G. A. H. Walker, Eds., May 1973.
2. G. A. H. Walker, J. R. Auman, V. Z. Buchholz, B. A. Goldberg, A. C. Gower, B. C. Isherwood, R. Knight and D. Wright: Application of an Image Isocon and Computer to Direct Digitization of Astronomical Spectra. Advances in Electron Physics, Vol. 33b, Academic Press, N. Y., 1972.
3. G. W. Goetze and A. H. Boerio: Secondary Electron Conduction (SEC) for Signal Amplification and Storage in Camera Tubes. Proc. IEEE 52, 1007, 1964.
4. P. M. Zucchini and J. L. Lowrance: Progress Report on Development of the SEC Vidicon for Astronomy. Astronomical Use of Television-Type Image Sensors, Proceedings of symposium at Princeton University, Princeton, N. J., May 1970, NASA SP-256.
5. D. McMullan and G. O. Towler: Some Properties of SEC Targets. Advances in Electronics and Electron Physics, Academic Press, N. Y., 1972, Vol. 33B.
6. N. P. Cumings and R. McIntosh, in preparation 1980.
7. R. J. Bray and R. E. Loughhead: Sunspots. John Wiley & Sons, Inc., New York, 1964.
8. D. G. Fink: Principles of Television Engineering. McGraw-Hill, New York, 1940.
9. J. A. Hall: Evaluation of Signal-Generating Image Tubes. Photoelectronic Imaging Devices, L. M. Biberman and S. Nudelman, eds., Plenum Press, N. Y., 1971.
10. W. A. Shurcliff: Polarized Light. Harvard University Press, Cambridge, MA, 1962.
11. W. Unno: Publ. Astronom. Soc. Japan 8, 109, 1956.
12. E. A. West: Applied Optics, 17, 3010, 1978.

APPROVAL

THE MSFC VECTOR MAGNETOGRAPH

By M. J. Hagyard, N. P. Cumings,
and E. A. West

The information in this report has been reviewed for technical content. Review of any information concerning Department of Defense or nuclear energy activities or programs has been made by the MSFC Security Classification Officer. This report, in its entirety, has been determined to be unclassified.



ERNEST HILDNER
Chief, Solar Sciences Branch



CHARLES R. CHAPPELL
Chief, Solar-Terrestrial Physics Division



CHARLES A. LUNDQUIST
Director, Space Sciences Laboratory